Map Uncertainties for Unmanned Underwater Vehicle Navigation Using Sidescan Sonar

J. Guo[1], W. H Wang[1], S. W. Huang[2], E. Chen[2] and F. C. Chiu[1]
[1]National Taiwan University, Department of Engineering Science and Ocean Engineering
No. 1, Sec.4, Roosevelt Road, Taipei, Taiwan, 10617, R.O.C.
[2] Taiwan Ocean Research Institute, Taipei, Taiwan, 10617, R.O.C.

***Abstract* - Navigation of unmanned underwater vehicle (UUVs) in unstructured environments without long baseline transponders is a challenging problem due to the lack of predefined sea floor landmarks. This study proposes a real time sea floor mapping method using sidescan sonar on UUVs. The mapping system combines the motion information and the observation model of the sidescan sonar. The observation process firstly detects environmental features and then localizes the feature positions relative to the UUV. The landmark localization procedure considers the working principle of sidescan sonar and the acoustic velocity in sea water to localize the landmark and calculate the sidescan sonar footprint region. An occupancy grid mapping algorithm is then used to map the sea floor combining the uncertainties of UUV's motion and measurement errors from the observations. This procedure was implemented on an UUV to verify its landmark detection capability. Experimental results conducted on sandy seabed with concrete targets are demonstrated.**

I. INTRODUCTION

Nowadays, sidescan sonar becomes common payloads for unmanned underwater vehicles (UUVs). A sidescan sonar produces a representation in image form of the seabed [1,2]. The sonar signals come from backscattering and reflection from sea floor are usually enhanced by time varying amplification gains. The resulting sidescan sonar images produce a representation of seafloor backscatterings, the imaging process can be simulated using bistatic models for building sidescan sonar simulators [3]. Sidescan sonar transmit signal in both vertical plane and horizontal plane and explore an area which is called "footprint" with different resolutions in the along-track direction and in the across-track direction. [4-6].

Sonar data can be used to classify the seabed property. Bell and Linnett used the Rayleigh distribution to verify their result of sidescan sonar simulation [3]. Dunlop pointed out the relationship between different distribution models on some assigned terrains which could be used to classify the seafloor [8]. Rayleigh, K-distribution and Nakagami distributions are the general statistical models to describe scattering signals and to classify the seabed. Constant false-alarm rate (CFAR) is a method to detect target signal within radar signals [7, 8] and communication system [9]. Study on using CFAR to detect targets was described in [10]. The use of CFAR combined with Target Presence Probability (TPP) was proposed to detect landmarks for the autonomous vehicles localization and mapping [11].

Information extracted from sidescan data offers a potential benefits to the navigation of UUVs in an unstructured environment. Sidescan sonar images of the seafloor typically consist of a series of scanlines, one per transmission-reception cycle, displayed perpendicularly to the survey track. A number of scanlines are necessary to make an image. To navigate an underwater vehicle with respect to a landmark, the landmark position has to be detected with high confidence. The range and resolution of sidescan sonar is subject to physical limitations, and noisy navigation sensors affect the accuracy of the motion of UUV [12, 13], Uncertainty is further created through algorithmic approximations. Target detection with sidescan image usually work offline. For navigation, it is important that UUVs capture the environment information in real-time. Previous works for underwater vehicle localization using sidescan sonar images can be found in [14-16]. Real time localization using sidescan images is still under investigation since the landmark images must be processed after collecting a certain amount of sea floor data which usually results in time delays in the navigation data. Thus, instead of using sidescan sonar for mapping the environment off-line, this work describes a procedure for mapping the sea floor and navigation using side-scan sonar scanline in real-time.

Processing navigation information in real-time is mostly a strict requirement on computation. Many popular algorithms are approximate, achieving timely responses through sacrificing accuracy [17]. One method to represent the uncertain environment caused by the sensors is to calculate the spatial relationships between the "features" observed by the sensor and the motion uncertainty, where the uncertain environment will be represented as a feature-based map [18]. Occupancy grids is a representation of an environment by an array of cells where each cell carries the belief of the state that it is occupied or empty [19, 20]. Moravec and Elfes accomplished the mapping problem by probabilistic framework such as Bayesian framework [21]. Thrun obtained grid maps by neural network based approach [22], where the inverse measurement model was obtained using binary Bayes filter and forward model approach [23]. In this work, the

978-1-4244-5222-4/10/$26.00 ©2010 IEEE

occupancy grids was chosen to describe the outcome of the detection to reduce the amount of target points and therefore, to reduce the computing time for the navigation.

This work investigates the gird-based mapping method to locate the sea floor target positions in real time for the unmanned underwater navigation. Scanlines' information instead of the sidescan images is processed to detect landmarks' position. The article is composed of five sections. Section II introduces the observation model of sidescan sonar and the mapping problem using the scanline information. Section III describes the detection technique. Section IV presents experimental results. Finally, concluding remarks are given in Section V.

II. MAPPING MODELING

A grid map proposed in this section could be constructed from scanlines and be updated co-currently while the new observation is obtained. The observation model gives a footprint which is a region ensonified by side-scan sonar. In addition, errors in the pitch, roll and yaw measurements of UUV affect the target's location uncertainty.

The occupancy grid mapping method generates a two-dimensional array of cells. Each cell is corresponding to a horizontal grid, and the size of the grid is the desired resolution. Each cell, C, has association with a variable $s(C)$. $s(C)$ is a discrete random variable with two states, occupied and empty. Besides, each cell contains a probabilistic estimate of its occupancy which is defined as $P(s(C)= occ)$ and $P(s(C)= emp)$, the probability of occupied cell and empty cell, respectively. Since the states are exclusive and exhaustive. Moreover, there could have several measurements associated with each grid cell. Given the sensor reading $z_{1:t}$ from side-scan sonar and the vehicle's pose $x_{1:t}$, the desired probability of the grid cell, this can be defined as conditional probability $P(s(C_i)=occ|z_{1:t},x_{1:t})$ and the estimation of the occupancy probability for each grid cell is now a binary estimation problem. A filter for this problem is the binary Bayes filter. The binary Bayes filter uses the log odds over the probability representation which avoids numerical instabilities for probabilities near zero or one. Therefore, the mapping problem of this work could be represent as

$$l_{t,i} = \log \frac{P(s(C_i) = occ \mid z_{1:t}, x_{1:t})}{1 - P(s(C_i) = occ \mid z_{1:t}, x_{1:t})} \tag{1}$$

The probabilities are easily recovered from log odds ratio:

$$P(s(C_i) = occ \mid z_{1:t}, x_{1:t}) = 1 - \frac{1}{1 + \exp\{l_{t,i}\}} \tag{2}$$

A function inverse_measurement_model was used to implement the inverse measurement model $P(s(C_i)=occ \mid z_t, x_t)$ in its log odds forms:

$$\begin{aligned} &\text{Inverse\_Measurement\_Model}(C_i=occ, x_t, z_t) \\ &= \log \frac{P(s(C_i)=occ \mid z_t, x_t)}{1\text{-}P(s(C_i)=occ \mid z_t, x_t)} \end{aligned} \tag{3}$$

which specifies the probability of occupancy of the grid cell $s(C_i)$ conditioned on the measurement z_t and vehicle's pose x_t. This probability constitutes an inverse sensor model, since it maps sensor measurements back to its causes.

The probability of the grid cell could be obtained by given the side-scan sonar observation and its navigation measurements. Due to the motion effects on the swathe, the target position should be corrected by the vehicle's pitch, roll

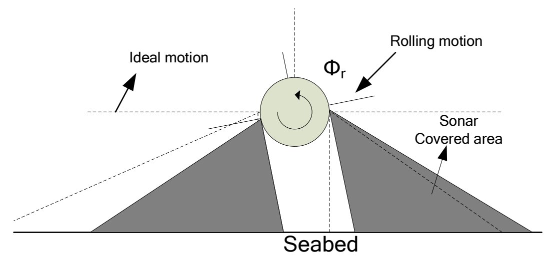

Fig. 1. Rolling effect. Φ_r is the roll angle of UUV.

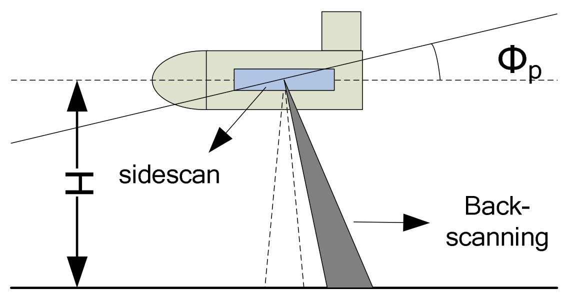

Fig. 2. Backscanning due to pitching of the vehicle. Φ_p is the roll angle of UUV.

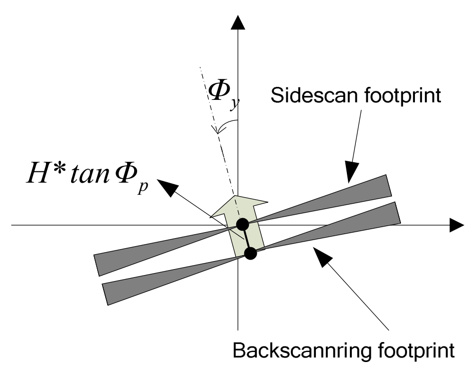

Fig. 3. Relative positions between the sidescan sonar scanning footprints with and without vehicle pitching. Φ_y is the roll angle of UUV.

and yaw angle before localizing the target position. Cobra indicated the situation caused by these three angles [12]. Figure 1 shows the rolling motion effect on the sonar coverage. The dashed line area indicates the coverage area with zero rolling angles and solid line represents area covered by the sonar when the vehicle rolls. The pitch angle causes the forward and the back scan as shown in Fig. 2. The dash line shows the vehicle swims horizontally and the solid line shows the backward scan with the angle Φ_p. The effect of pitch on sonar footprint positions is shown in Fig. 3. After correcting the vehicle motion and slant, every detected target has a relative coordinate point which is related to the center of UUV. The position of the target can be represented by [13]

$$\begin{bmatrix} x' \\ y' \\ H' \end{bmatrix} = T * \begin{bmatrix} x \\ y \\ H \end{bmatrix} \tag{4}$$

where (x, y) are the position relative to the center of the UUV, x is the across-track direction, y is the along-track direction, (x', y') are the corrected position, H represents the vehicle height from the sea floor and can be obtained by:

$$H = T_b\left(C/2\right) \tag{5}$$

where T_b is the time of the first return of the sonar beam, C is the speed of sound in the water. A general transformation T involving all three rotations requires an ordering convention for it to be unique. In order to preserve the uniqueness of the coordinate system, performing yaw then pitch then roll transformations, we have the general transformation:

$$T = \begin{bmatrix} c\Phi_y c\Phi_r & c\Phi_r s\Phi_y & s\Phi_r \\ s\Phi_p s\Phi_r c\Phi_y - c\Phi_p s\Phi_y & s\Phi_p s\Phi_y s\Phi_r - c\Phi_p c\Phi_y & -s\Phi_p c\Phi_r \\ -c\Phi_p s\Phi_r c\Phi_y - s\Phi_p s\Phi_y & -c\Phi_p s\Phi_y s\Phi_r + s\Phi_p c\Phi_y & c\Phi_p c\Phi_r \end{bmatrix} \tag{6}$$

where c is cosine and s is sine. Φ_y is the heading angle of the vehicle, Φ_p is the pitch angle when bow up is positive, Φ_r is the roll angle when port up is positive. Usually, the information comes from the navigation sensors are with noises, so the noisy data would influence the localization of the target. The position of the UUV's center relative to the global coordinate is shown as follows:

$$X_{g1} = [x_{g1} \;\; H_{g1} \;\; y_{g1} \;\; \Phi_{pg1} \;\; \Phi_{yg1} \;\; \Phi_{rg1}]^{\mathrm{T}} \tag{7}$$

where x_{g1}, H_{g1} and y_{g1} are the location of UUV in global coordinate. Φ_{pg1}, Φ_{yg1} and Φ_{rg1} are the included angles of UUV of three axis in global coordinate. Assume that the error of the UUV's position have Gaussian distributions, the covariance matrix can then be shown as follows:

$$C_{g1} = diag\left(\sigma_{x_{g1}}{}^2, \sigma_{y_{g1}}{}^2, \sigma_{H_{g1}}{}^2, \sigma_{\Phi_{pg1}}{}^2, \sigma_{\Phi_{yg1}}{}^2, \sigma_{\Phi_{rg1}}{}^2\right) \tag{8}$$

where the diagonal terms are the standard deviation relative to each component in X_1.

The target position relative to the center of UUV is shown as follows:

$$X_{12} = [x_{12} \;\; y_{12} \;\; H_{12} \;\; \Phi_{p12} \;\; \Phi_{y12} \;\; \Phi_{r12}]^{\mathrm{T}} \tag{9}$$

where x_{12} is the horizontal range of the target relative to the UUV center, which is shown as follows:

$$x_{12} = \sqrt{R_{12}{}^2 - H_{12}{}^2} \tag{10}$$

R_{12} is the slant range derived from the sidescan return, and H_{12} is the height of the UUV. In addition, the term y_{12} is the distance in along-track direction relative to the center of UUV, and y_{12} is zero. The three angles of the target relative to the center of UUV could be obtained as follows:

$$\begin{bmatrix} \Phi_{p12} \\ \Phi_{y12} \\ \Phi_{r12} \end{bmatrix} = \begin{bmatrix} \mathrm{atan2}(H_{12}, y_{12}) \\ \mathrm{atan2}(y_{12}, x_{12}) \\ \mathrm{atan2}(H_{12}, x_{12}) \end{bmatrix} = \begin{bmatrix} 0 \\ 0 \\ \mathrm{atan2}(H_{12}, x_{12}) \end{bmatrix} \tag{11}$$

where Φ_{p12} is the include angle of x axis relative to the UUV. Besides, Φ_{y12} and Φ_{r12} are the included angles of z axis and y axis relative to the UUV. The across-track resolution and the along-track resolution would vary with the slant range. Therefore, assume the resolutions is the standard deviation of target position relative to the UUV in x and y direction. The covariance matrix is shown as follows:

$$C_{12} = diag\left(\sigma_{x_{12}}{}^2, \sigma_{y_{12}}{}^2, \sigma_{H_{12}}{}^2, \sigma_{\Phi_{p12}}{}^2, \sigma_{\Phi_{y12}}{}^2, \sigma_{\Phi_{r12}}{}^2\right) \quad (12)$$

where the diagonal terms are shown as follows:

$$\begin{bmatrix} \sigma_{x_{12}}{}^2 \\ \sigma_{y_{12}}{}^2 \\ \sigma_{H_{12}}{}^2 \\ \sigma_{\Phi_{p12}}{}^2 \\ \sigma_{\Phi_{y12}}{}^2 \\ \sigma_{\Phi_{r12}}{}^2 \end{bmatrix} = \begin{bmatrix} \left(\frac{1}{2} \bullet \frac{CT_d}{2\sin(\theta)}\right)^2 \\ \left(\frac{1}{2} \bullet R\varphi\right)^2 \\ 0 \\ 0 \\ 0 \\ 0 \end{bmatrix} \quad (13)$$

where θ is the incident angle, φ is the aperture of the directivity lobe in the horizontal plane. R denotes the slant range of a target, and T_d is the transmitted time (pulse duration) of the side scan sonar. To combine the uncertainties out of motion sensors and uncertainties out of side-scan sonar measurements, the target position coordinate relative to the global coordinate could be established by:

$$X_{g2} = \begin{bmatrix} x_{g2} \\ y_{g2} \\ H_{g2} \\ \Phi_{pg2} \\ \Phi_{yg2} \\ \Phi_{rg2} \end{bmatrix} \triangleq X_{g1} \oplus X_{12} \quad (14)$$

The symbol $\oplus$ indicates the compounding of vectors. The terms x_{g2}, y_{g2} and H_{g2} are the location of the target relative to the global coordinate shown as follows:

$$\begin{bmatrix} x_{g2} \\ y_{g2} \\ H_{g2} \end{bmatrix} = T_{g1} \begin{bmatrix} x_{12} \\ y_{12} \\ H_{12} \end{bmatrix} + \begin{bmatrix} x_{g1} \\ y_{g1} \\ H_{g1} \end{bmatrix} = \begin{bmatrix} x'_{12} \\ y'_{12} \\ H'_{12} \end{bmatrix} + \begin{bmatrix} x_{g1} \\ y_{g1} \\ H_{g1} \end{bmatrix} \quad (15)$$

and Φ_{pg2}, Φ_{yg2} and Φ_{rg2} are the included angles relative to the global coordinate:

$$\begin{bmatrix} \Phi_{pg2} \\ \Phi_{yg2} \\ \Phi_{rg2} \end{bmatrix} = \begin{bmatrix} \text{atan2}(H'_{12}, y'_{12}) \\ \text{atan2}(y'_{12}, x'_{12}) \\ \text{atan2}(H'_{12}, x'_{12}) \end{bmatrix} \quad (16)$$

The term T_{g1} is the rotation matrix which could be obtained from Eq. 6. The covariance of this relationship could be obtained by using the Jacobian for estimation as follows:

$$C_{g2} \approx J_{1\oplus} C_{g1} J_{1\oplus}^T + J_{2\oplus} C_{12} J_{2\oplus}^T \quad (17)$$

The term C_{g2} is the first order estimate of the covariance matrix representing the distribution of the target point position relative to the global coordinate. Besides, $J_{1\oplus}$ and $J_{2\oplus}$ are the left and right halves (6×6) matrices of the compounding Jacobian (6×12):

$$J_{\oplus} = \begin{bmatrix} J_{1\oplus} & J_{2\oplus} \end{bmatrix} \quad (18)$$

$$J_{\oplus} \triangleq \frac{\partial(X_{g1} \oplus X_{12})}{\partial(X_{g1}, X_{12})} = \frac{\partial(X_{g2})}{\partial(X_{g1}, X_{12})} \quad (19)$$

Figures 4 and 5 show the result of inverse measurement model, the covariance represented by an ellipse was obtained from Eq. 17. Once the detection result is with target present, the algorithm will return the log probability of the cell. Also, the log probability will be obtained if detection result indicates target absence. Otherwise, if the cell is outside of the region of footprint, this model will assign to this cell with a prior probability value.

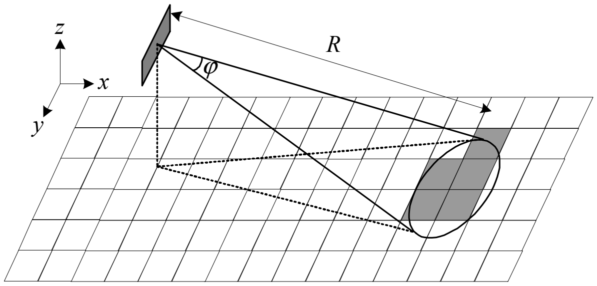

Fig. 4. The geometry of measurement uncertainty for long slant ranges. The across-track resolution is smaller than the along-track resolution.

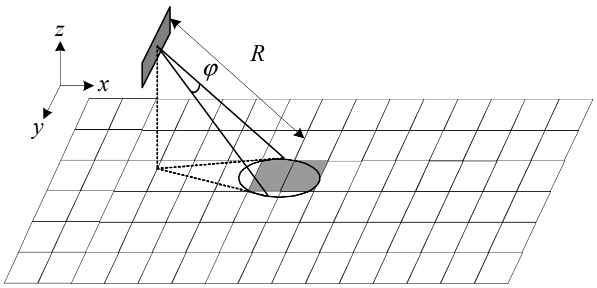

Fig. 5. The geometry of measurement uncertainty for short slant ranges. Unlike the case shown in Fig. 4, the across-track resolution is larger than the along-track resolution.

III. DETECTION METHOD

The purpose of target detection is to determine the probability of the target location in the scanline. When the seabed is not flat, geometrical correction requires a priori assumptions about the topography or additional recording of bathymetry (possibly obtained by the side-scan sonar itself, if it is equipped with an interferometer). To reduce computing time, downsampling was performed to reduce the data quantity. Each received scanline was downsampled and quantity of data was reduced to one tenth of the original one. Normalizing the scanline data reduces the effect of the terrains and obtains higher detection rate. Normalization also maintains the ambient level in the same level for the detection purpose.

The major function of the detector is to distinguish the difference between known seabed from uncertain ones. The detection algorithm extracts features from the sonar data according to parameters of their pre-selected features. Log-energy, distribution parameters and the error between estimation distribution and histogram are the most common features that were employed to design seafloor classifiers [8, 24]. Data processing steps of the detector are shown in Fig. 6. Three features are extracted from scanline data, and a Bayesian classifier is employed to determine the signal class.

A naïve Bayesian classifier is a simple probabilistic classifier based on Bayes' theorem and naïve assumption. In naïve assumption, it is assumed that attributes are all independent. Classify any new datum instance $x=(F_1,\ldots F_t)$ as:

$$h_{Naive\ Bayes} = \underset{h\in[yes,no]}{\arg\max} \frac{P(h)P(x\mid h)}{p(x)} \tag{20}$$

where $P(\square)$ is the probability function and h is maximum likelihood hypothesis. Since the evidence is a constant if the values of the feature variables are known, Eq. 20 can be further represented as:

$$h_{Naive\ Bayes} = \underset{h\in[yes,no]}{\arg\max}\, C * P(h)\prod_t P(F_t \mid h) \tag{21}$$

C is constant in Eq. 21. Moreover, Eq. 21 can be represented as Eq. 22.

$$\begin{aligned} h = C * \arg\max\{&P(T_p) * P(F_1,F_2,F_3 \mid T_p), \\ &P(T_{ab}) * P(F_1,F_2,F_3 \mid T_{ab})\} \end{aligned} \tag{22}$$

where $P(T_p)$ denotes the probability of target presence and $P(T_{ab})$ is the probability of target absence. F_1 is the log-energy value, F_2 is the distribution shape parameter and distribution error is F_3.

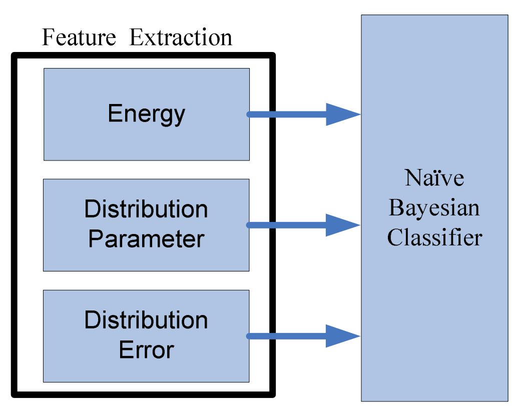

Fig. 6 Detector signal processing diagram.

TABLE I

Detection performance

Parameters	T_p Error (Actual T_{ab})	T_{ab} Error (Actual T_p)	Total Error
F_1&F_2	20	24	44
F_2&F_3	26	19	45
F_1&F_3	15	19	34
F_1&F_2&F_3	9	24	33

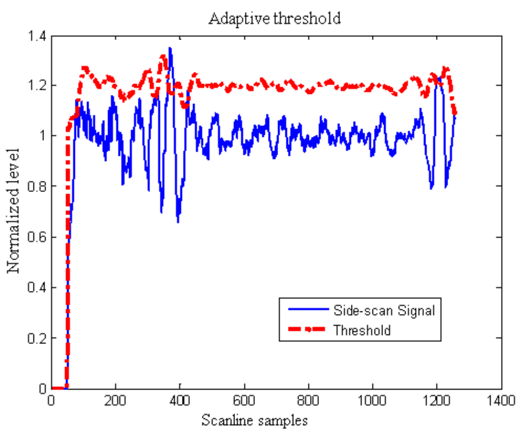

Fig. 7 Threshold performance with no target in signal.

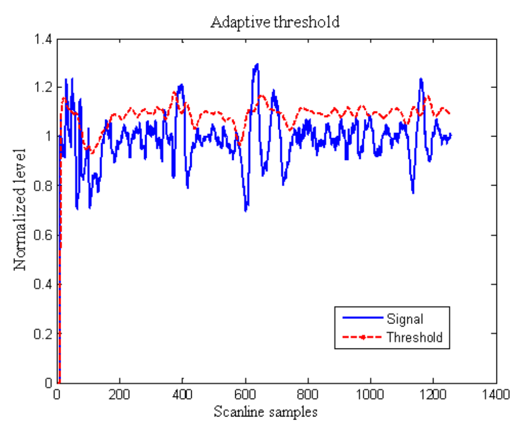

Fig. 8 Thresholding performance with target in signal.

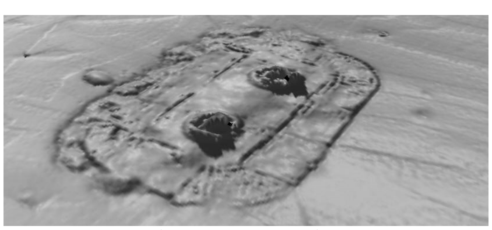

Fig. 9 Target overview

TABLE II

Side-scan sonar specifications

Specification	Description
Operation Frequency	400 KHz
Scan rate	5 Hz
Sampling interval	15360 Nanosecond
Pixels in each scanline	12574
Slant range	145 m
Pulse interval	0.1 ms
Horizontal Beam Width	0.4º
Yaw/Pitch/Roll	Yaw Accuracy: < 1.5 º RMS Roll, Pitch Accuracy: ± 0.4 º

Table I compares the results of detection errors using two-feature combinations with that of three features. It demonstrates the detector performs well with three features and the performance was degraded using any two combinations of features. Thresholding is used for signal segmentation. Constant thresholding for detecting target features in a signal may fail due to the noises. Adaptive thresholding has the advantage as the threshold value can be adjusted according to the noise level in the signal. The concept of Constant False Alarm Rate (CFAR) was extensively employed in Radar signal processing field. This study uses an adaptive threshold algorithm based on CFAR to find out the target in the complex background. Figures 7 and 8 show the scanline signals with target and without target information, respectively. The target can be shown to be detected by the adaptive thresholding.

IV. EXPERIMENTS

The image of the target object on the seafloor is shown in Fig. 9. The target image was generated by a multi-beam sonar. The environmental background was a sandy seabed and the dimension of target is approximately 100 meters by 150 meters. The sidescan sonar parameters were listed in Tab. II. The vehicle was piloted with pre-planned paths over the target area while collecting the side-scan data.

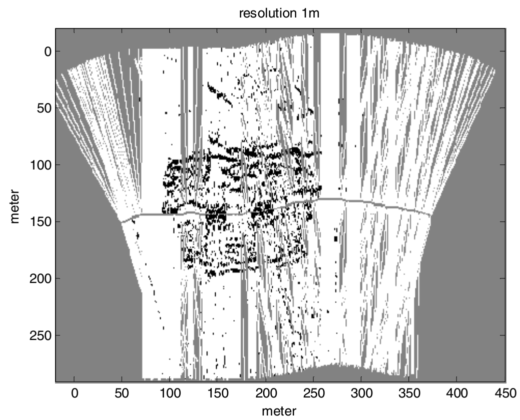

Fig. 10 Grid map constructed by treating scanlines with no uncertainties. No compensation on the effects of the pitch, roll and yaw.

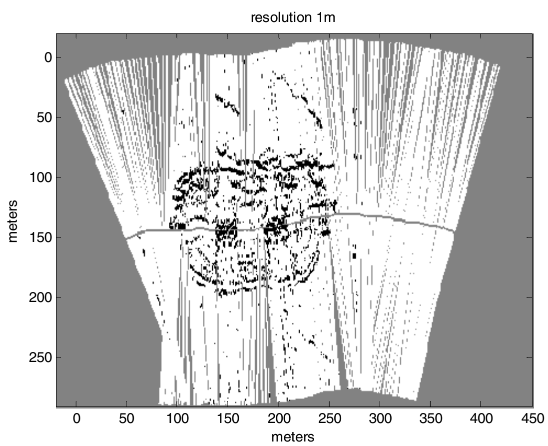

Fig. 11 Grid map constructed by treating scanlines with no uncertainties. Effects of the pitch, roll and yaw were considered to correct the map. Map distortions are less than that shown in Fig. 10.

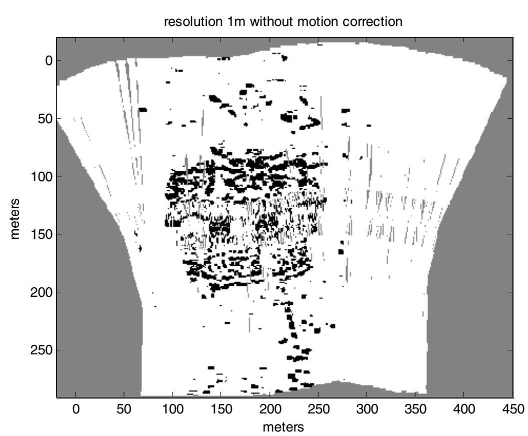

Fig. 12 Grid map constructed by treating scanlines with uncertainties. Effects of the pitch, roll and yaw were not considered to correct the map. Map distortions are less than that shown in Fig. 10. More grid areas were covered by scanlines.

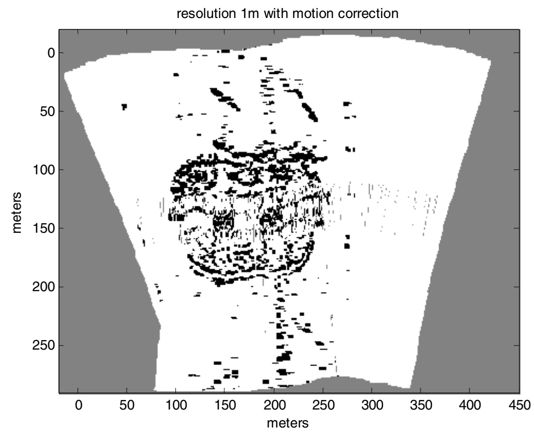

Fig. 13 Grid map constructed by treating scanlines with uncertainties. Effects of the pitch, roll and yaw were considered to correct the map. Map distortions are less than those shown in Figs. 10 to 12. Most grid areas were covered by scanlines.

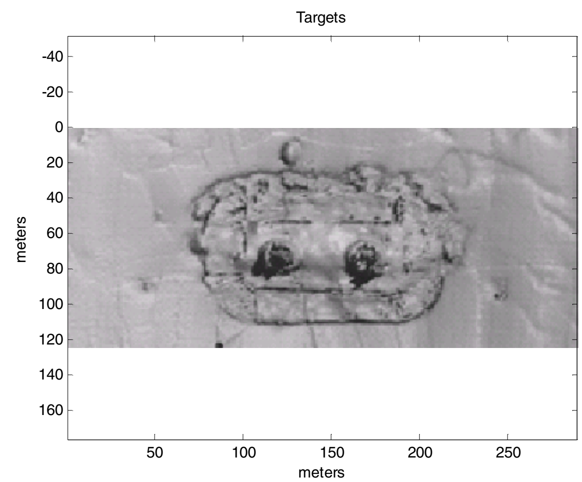

Fig. 14 True map constructed by mutlibeam sonar.

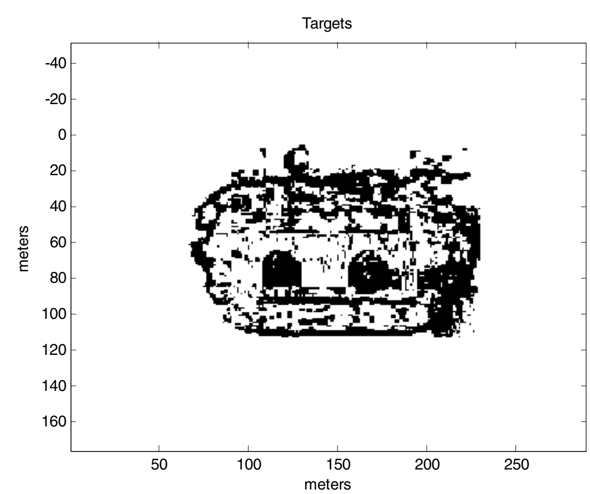

Fig. 15 Occupancy grid map constructed out of the true map.

Figures 10 and 12 are the mapping result without taking the motion uncertainties into account. Figure 10 shows that the mapping without motion correction using grid resolution of 1 meter. The grid map displayed distortions at the occupied area. Figures 11, 13 show the mapping result with UUV's motion correction using the same grid resolution. Obviously, the distortions were reduced by correcting motion effects. The far range of occupied areas displayed larger errors than the near range of occupied areas. Figure 14 is the true size of the targets constructed by a mutlibeam sonar, and Fig. 15 is the occupancy map constructed out of the true map. The accuracy of mapping is obtained by calculating a correlation coefficient of true map and resultant map. Correlation coefficients were obtained by Eq. 23, using GPS position to align the occupancy map of the true map with maps generated by the sidescan sonar.

$$\rho_{m_1,m_2} = \frac{\operatorname{cov}(m_1,m_2)}{\sigma m_1 \sigma m_2} = \frac{E(m_1 m_2) - E(m_1)E(m_2)}{\sqrt{E(m_1{}^2) - E^2(m_1)}\sqrt{E(m_2{}^2) - E^2(m_2)}} \quad (23)$$

where m_1 and m_2 are the grid map of true map and the sidescan sonar generated map. Table III lists the correlation coefficient of the grid maps of Fig.10 to 13 with respect to the true map. It indicates that compensating the effect of UUV motion has significant effect in reducing the map distortion. Furthermore, compounding the uncertainties of side-scan sonar and the uncertainties of UUV's motion sensors, the resulting map is much more accurate than considering only the UUV's motion effects. Figure 16 indicates the variation of targets uncertainties with different slant range and the uncertainties compounded by the side-scan sonar uncertainty with UUV motion uncertainties. The detail of the range 1 to 5 uncertainties are shown in Figs. 17 to 21. Figure 17 shows the uncertainties of left scanline in the nearest slant range. As mentioned before, the uncertainties of side-scan sonar are the defined as the footprint resolutions. In Fig.17, the solid ellipse is the uncertainty of the target caused by the footprint of side-scan sonar, and the uncertainty in across-track direction are larger than in along-track direction. From Fig. 17 to Fig. 21, the solid ellipse is getting larger in along-track direction and smaller in across track-direction. In addition, the dotted ellipse is the uncertainties compounded by the side-scan sonar uncertainty with UUV motion uncertainties. Due to fact that noises in yaw is larger than pitch and roll, the dotted ellipse is getting larger in along-track direction than in across-track direction with longer slant range. Uncertainties in the right scanline exhibit the similar phenomenon as that in the left scanline.

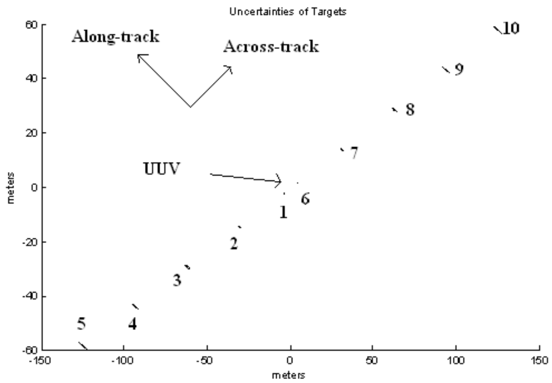

Fig. 16 The uncertainties of targets with different slant range in a scanline. This Figure indicates the variation of targets uncertainties with different slant ranges and the uncertainties compounded by the side-scan sonar uncertainty with UUV motion uncertainties. The details of ranges 1 to 5 uncertainties are shown in Figs. 15 to 19.

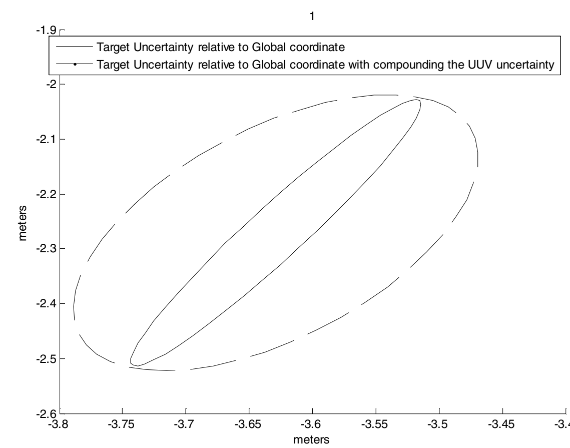

Fig. 17 Uncertainties of target at range 1 near by the UUV of left scanline. The solid ellipse is the target uncertainties caused by the error of side-scan sonar. The dotted ellipse is the target uncertainties compounded by the side-scan sonar uncertainty with UUV motion uncertainties.

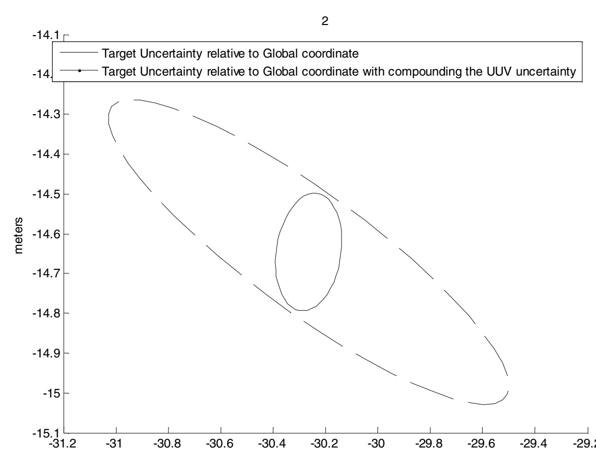

Fig. 18 Uncertainties of target at the range 2 of the left scanline.

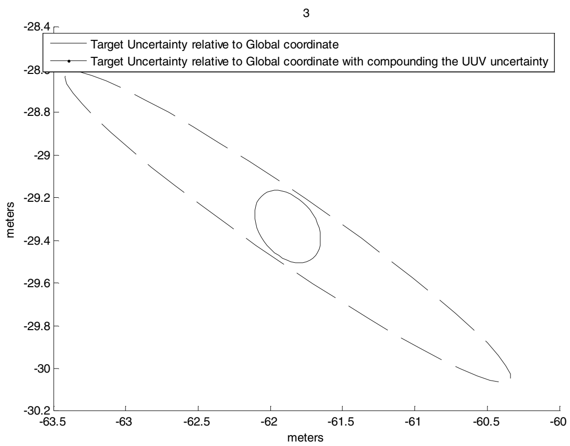

Fig. 19 Uncertainties of target in at the range 3 of the left scanline.

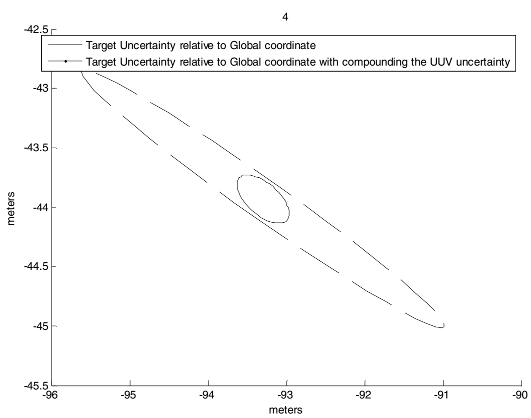

Fig. 20 Uncertainties of target at the range 4 in the left scanline.

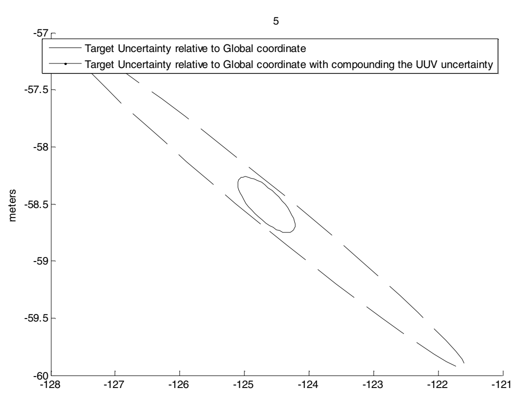

Fig. 21 Uncertainties of target at the range 5 of the left scanline.

TABLE III

Grid map correlation with respect to the true map. Similarity to the true map is indicated by the value of the correlation coefficient.

Figure number	UUV Motion correction	Covariance compounded by the side-scan sonar uncertainty with UUV motion uncertainties	Map similarity correlation coefficient
Fig. 10	No	No	0.248
Fig. 11	Yes	No	0.306
Fig. 12	No	Yes	0.302
Fig. 13	Yes	Yes	0.417

V. CONCLUSION

This study proposes a real time sea floor mapping method using sidescan sonar for UUVs. The mapping system combines the UUV motion information and the observations of side-scan sonar. The observation model of side scan sonar describes detection and target localization with respect to the UUV and the global coordinate. Detection was achieved based on processing the sidescan sonar scanline in real-time. The target localization procedure localizes the target and calculates the footprint region of the side-scan sonar. Finally, the occupancy grid mapping algorithm was used to map the sea floor combining the uncertainties of UUV's motion and measurement from the side-scan sonar. In the future work, experimental techniques in mapping and self-localization of UUVs will be studied in sea areas that have unknown underwater features.

ACKNOWLEDGMENT

The author would like to thank the National Science Council of the Republic of China, Taiwan, for financially supporting this research under Contract No. NSC95-3114-E002-001.

REFERENCES

[1] J. P. Fish, "Sound Underwater Images," American Underwater Search and Survey, Ltd, 1990

[2] Klein, *Side Scan Sonar Record Interpretation*, Klein1associates Inc., 1985

[3] J.M. Bell and L.M. Linnett, "Simulation and Analysis of Synthetic Sidescan Sonar Images," *IEE Proceedings -Radar, Sonar and Navigation*, vol. 144, no 4, pp.219-226, August 1997.

[4] X. Lurton, *An Introduction to Underwater Acoustics. Principles and Applications*, London(Springer), 2002

[5] H. Medwin, "Speed of Sound in Water: A Simple Equation for

Realistic Parameters," *Journal of the Acoustical Society of America*, 58, 1318-1319, 1975.

[6] C. T. Chen, F. J. Millero, "Speed of Sound in Sea Water at High Pressures," *Journal of the Acoustical Society of America*, 62, 1129-1135, 1977.

[7] J. Dunlop, "Statistical Modelling of Sidescan Sonar Images," *OCEANS '97. MTS/IEEE Conference Proceedings*, vol.1, pp.33-38, 1997.

[8] H. Rohling, "Radar CFAR Thresholding in Clutter and Multiple Target Situations," *IEEE Transactions on Aerospace and Electronic Systems*, vol.ASE-19, 1983.

[9] P.P. Gandhi and S.A. Kassam, "Analysis of CFAR Processors in Nonhomogeneous Background," *IEEE Transactions on Aerospace and Electronic Systems*, vol.24, 1988.

[10] Q. Jiang, S. Wang, D. Ziou, A.E. Zaart, G.B. Benie, M.T Rey, and M. Henschel, "Ship Detection in RADARSAT SAR Imagery," *1998 IEEE International Conference on Systems, Man, and Cybernetics*, vol.5, pp.4562-4566, 1998.

[11] H.G. Kim, I. Song, S.Y. Kim, J.H. Lee, and S.C. Kim, "Adaptive Code Acquisition Using A Go-CFAR Processor In DS/CDMA Systems," *IEEE TENCON 99*, vol.1, pp.542-545, 1999.

[12] D.T Cobra, A.V Oppenheim, and J.S.Jaffe, "Geometric Distortions in Side-Scan Sonar Images: A Procedure for Their Estimation and Correction," *IEEE Journal of Oceanic Engineering*, vol.17, pp.252 – 268, 1992.

[13] S.D. Anstee "The Effects of Towfish Motion on Sidescan Sonar Images," *MRL Research Report*, Department of Defence DSTO Materials Research Laboratory, 1994.

[14] I. Tena Ruiz, S. Reed, Y. Petillot, and D.M. Lane "Concurrent Mapping and Localization Using Sidescan Sonar," *IEEE Journal of Oceanic Engineering*, vol.29, pp.442 – 456, 2004.

[15] B. Zen, G. Mailfert, A. BerthoIom, and H. Ayreault, "Sidescan Sonar Image Processing for AUV Navigation," *Oceans 2005 – Europe*, vol.1, pp. 124-130, 2005.

[16] D.R. Carmichael, L.M. Linnett, S.J. Clarke, and B.R. Calder, "Seabed Classification Through Multifractal Analysis of Sidescan Sonar Imagery," *Inst. Elect. Eng. Radar, Sonar, Navigation*, no.3, pp. 140-148, 1996.

[17] S. Thrun, W. Burgard, D. Fox, *Probabilistic Robotics*, MIT Press, Cambridge, MA, 2005.

[18] R. Smith, M. Self, P. Cheeseman, "Estimating Uncertain Spatial Relationships in Robotics," *in Proceedings of Uncertainty in Artificial Intelligence,* Philadelphia, PA, PP. 267-289, Aug. 1986.

[19] H. Moravec, A. Elfes, "High Resolution Maps from Wide Angle Sonar," *in Proceedings of the 1985 IEEE International Conference on Robotics and Automation*, 1985

[20] A. Elfes, "Using Occupancy Grids for Robot Perception and Navigation," *Computer Magazine*, June 1989, pp. 46-57.

[21] L. Matthies, A. Elfes, "Integration of Sonar and Stereo Range Data Using a Grid-based Representation, " *Proceedings of the 1988 IEEE International Conference on Robotics and Automation*, PA, USA, 1988..

[22] S. Thrun, "Exploration and Model Building in Mobile Robot Domains," *in Proceedings of IEEE International Conference on Neural Networks*, Seattle, Washington, USA: IEEE neural Network Council, 1993, pp. 170-180.

[23] S. Thrun, "Learning Occupancy Grids with Forward Sensor Models," *Autonomous Robots* 15, 111-127, 2003

[24] B. Atal and L. Rabiner, "A Pattern Recognition Approach to Voiced-unvoiced-silence Classification with Applications to Speech Recognition," *IEEE Transactions on Acrostics, Speech, and Signal Processing*, vol. ASSP-24, no 3, June 1976.